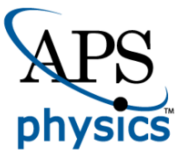

Quadrupole Collectivity in Neutron-Rich Fe and Cr Isotopes

H. L. Crawford *et al.*

Phys. Rev. Lett. **110**, 242701 — Published 13 June 2013

DOI: 10.1103/PhysRevLett.110.242701

Quadrupole Collectivity in Neutron-Rich Fe and Cr Isotopes

H. L. Crawford[1], R. M. Clark[1], P. Fallon[1], A. O. Macchiavelli[1], T. Baugher[2,3], D. Bazin[2], C. W. Beausang[4], J. S. Berryman[2], D. L. Bleuel[5], C. M. Campbell[1], M. Cromaz[1], G. de Angelis[6], A. Gade[2,3], R. O. Hughes[4], I. Y. Lee[1], S. M. Lenzi[7], S. Paschalis[1], M. Petri[1], A. Poves[8], A. Ratkiewicz[2,3], T. J. Ross[4], E. Sahin[6], D. Weisshaar[2], K. Wimmer[2,9], and R. Winkler[2]

[1] *Nuclear Science Division, Lawrence Berkeley National Laboratory, Berkeley, California 94720, USA*

[2] *National Superconducting Cyclotron Laboratory, Michigan State University, East Lansing, Michigan 48824, USA*

[3] *Department of Physics and Astronomy, Michigan State University, East Lansing, Michigan 48824, USA*

[4] *University of Richmond, Richmond, Virginia 23173, USA*

[5] *Lawrence Livermore National Laboratory, Livermore, California 94551, USA*

[6] *Laboratori Nazionali di Legnaro, INFN, Legnaro (PD), Italy*

[7] *Dipartimento di Fisica dell'Università and INFN, Sezione di Padova, I-35131 Padova, Italy*

[8] *Departamento de Física Teórica e IFT-UAM/CSIC, Universidad Autónoma de Madrid, E-28049 Madrid, Spain and*

[9] *Department of Physics, Central Michigan University, Mount Pleasant, Michigan 48859, USA*

(Dated: May 22, 2013)

Intermediate-energy Coulomb excitation measurements have been performed on the $N \geq 40$ neutron-rich nuclei ^{66,68}Fe and ^{64}Cr. The reduced transition matrix elements, providing a direct measure of the quadrupole collectivity, $B(E2; 2_1^+ \rightarrow 0_1^+)$, are determined for the first time in $^{68}\mathrm{Fe}_{42}$ and $^{64}\mathrm{Cr}_{40}$, and confirm a previous RDM lifetime measurement in $^{66}\mathrm{Fe}_{40}$. The results are compared to state of the art large-scale shell-model calculations within the *fpgd* model-space using the LNPS effective interaction, and confirm the results of the calculations that show these nuclei are well deformed.

PACS numbers: 25.70.De, 27.40.+e

For many decades the nuclear shell structure originally proposed by Mayer, Jensen and co-workers [1, 2], where energy gaps are predicted at specific nucleon numbers, was a paradigm of nuclear physics, as it was consistent with the experimental findings at or near the valley of beta-stability. However, with the possibility of producing more exotic nuclei, the traditional magic numbers have been observed to be weakened, or to disappear while new sub-shell gaps have emerged. In particular, the role of the proton-neutron tensor interaction has been recognized as driving changes in shell structure [3]. Alterations to the effective single-particle orbital gaps can lead to enhanced particle-hole excitations, which are supported by deformation and pairing effects, and may give rise to new regions of well-developed nuclear deformation.

A region of recent interest is that of the neutron-rich isotopes near N=40, below the $_{28}$Ni isotopes. In many ways structurally similar to the 'island of inversion' nuclei near N=20 [4], the Fe and Cr isotopes in this region have been experimentally observed to exhibit increasingly collective behaviour, rather than the near-magic behaviour naïvely expected assuming a robust N=40 sub-shell gap. In a schematic way, the development of collectivity moving from $_{28}$Ni to $_{26}$Fe and $_{24}$Cr is understood as a result of a narrowing of the N=40 sub-shell closure and the enhancement of quadrupole collectivity through promotion of neutron pairs across the sub-shell gap. With the removal of protons from the $1f_{7/2}$ orbital, the attractive tensor and central parts of the p-n interaction between $1f_{7/2}$ proton holes and neutrons in the $1g_{9/2}$ and $2d_{5/2}$ orbits pulls these neutron single-particle levels down in energy. At the same time, the repulsive tensor $(\pi 1f_{7/2})^{-1} - \nu 1f_{5/2}$ interaction dominates over the central attractive p-n interaction, and drives the neutron $1f_{5/2}$ orbital up, effectively quenching the N=40 gap. Looking at it another way, adding twelve neutrons to ^{48}Ca produces a gapless ^{60}Ca; as protons are added in the $1f_{7/2}$ orbit the repulsive interaction between the $1f_{7/2}$ protons and the $1g_{9/2}$ and $2d_{5/2}$ neutrons and the strongly attractive $\pi 1f_{7/2}$-$\nu 1f_{5/2}$ interaction opens the N=40 gap up to its value in ^{68}Ni. The disappearance of the N=40 gap towards ^{60}Ca supports the structural energy gain achieved by neutrons occupying the low-Ω substates of the $1g_{9/2}$ orbital, where Ω is the projection of the total angular momentum onto the symmetry axis [5], which drives the system towards deformed, collective structures. In other words, the quadrupole collectivity of the systems in the region is enhanced as a result of the nearby presence of the Δj=2 partner orbitals $1\nu g_{9/2}$ and $2\nu d_{5/2}$, members of a quasi-SU(3) sequence, which is known to generate quadrupole collectivity [6].

The picture of structural evolution described above is borne out by calculations using state-of-the-art large-scale shell model calculations [7]. While the details of the predictions for the degree of collectivity vary between theoretical approaches, all available predictions place the mid-shell $^{64}_{24}$Cr nucleus at the center of the region of collectivity near N=40. In this nucleus, defor-

mation is maximized not only by the increased population of the $g_{9/2}$ and $d_{5/2}$ neutron orbits, but also by the strong proton-neutron correlations which develop with four active protons in the fp shell [7]. However, as is pointed out by Baugher *et al.* [8], this maximum in deformation may not be completely robust, as they predict a saturation in deformation already reached in ^{62}Cr. The primary motivation of this work is the first direct measurement of the collectivity of the key nucleus, ^{64}Cr.

Early measurements of the energy of the first 2^+ excited states in the Fe and Cr isotopes [9–12] showed a decreasing trend through N=40, and recent lifetime measurements in the neutron-rich ^{64,66}Fe isotopes up to N=40 [13, 14] have confirmed the collectivity in the Fe isotopes. In the lighter Cr isotopic chain, data are limited for $N \geq$40. Coulomb excitation measurements provided collectivity data at N=32 and 34 in the Cr isotopes [15]. The first (indirect) confirmation of increasing collectivity up to N=38 was provided by proton inelastic scattering measurements [16], recently confirmed by intermediate-energy Coulomb excitation, probing the $B(E2)$ values directly [8]. However in $^{64}_{40}$Cr the only experimentally available information is E(2^+_1) and E(4^+_1) [10]; no measure of the extent of collectivity is reported in the literature.

In addition to this first direct measurement of the collectivity of $^{64}_{24}$Cr, we also present here confirmation of the measured quadrupole collectivity in ^{66}Fe [14] and an extension of the $B(E2)$ systematics in the $_{26}$Fe isotopic chain to ^{68}Fe at N=42. Quadrupole collectivity was measured via determination of the $B(E2: 0^+_1 \rightarrow 2^+_1)$ or reduced transition matrix elements, using intermediate-energy Coulomb excitation [17]. The measured $B(E2: 0^+_1 \rightarrow 2^+_1)$ values in ^{66,68}Fe and ^{64}Cr are compared with large-scale shell-model calculations, providing a test of theory at the center of this new "island of inversion".

The measurements were performed at the National Superconducting Cyclotron Laboratory (NSCL) at Michigan State University. Secondary radioactive ion beams containing ^{66}Fe, ^{68}Fe and ^{64}Cr were produced by in-flight fragmentation of a 130-MeV/A ^{76}Ge primary beam on a 399 mg/cm^2 ^{9}Be foil production target. The fragments of interest were selected in the A1900 fragment separator [18], using three separate magnetic rigidity settings for the three isotopes studied. In all cases, a 240 mg/cm^2 achromatic aluminum wedge degrader was located at the object position of the fragment separator, and the total momentum acceptance was restricted to 2%. The resulting rare isotope beams had purities of 23% for ^{66}Fe, 6% for ^{68}Fe and 2% for ^{64}Cr, with average rates of approximately 300, 20 and 2 particles per second incident on target respectively.

Bismuth targets used to induce projectile Coulomb excitation were located at the target position of the S800 spectrograph [19] in the S3 experimental vault. Coulomb excitation of ^{66}Fe was studied using ^{209}Bi targets of two thicknesses, 245.2 mg/cm^2 and 492 mg/cm^2. Coulomb excitation of ^{68}Fe was studied with a target thickness of 245.2 mg/cm^2, while the measurement for ^{64}Cr used the thicker target of 492 mg/cm^2. The identification of the reaction residues was performed on an event-by-event basis utilizing the detection systems of the S800 focal plane [20]. Energy loss was measured in an ionization chamber, while two xy-position sensitive cathode-readout drift chambers (CRDCs) provided position and angle information, and a plastic timing scintillator provided a stop for the time-of-flight measurement. Position and angle information at the target position was reconstructed using the information from the focal plane CRDCs, together with ion optics information for the S800. Reconstruction of the scattering angle on an event-by-event basis was critical to ensure selection of 'safe' Coulomb excitation interactions. In intermediate-energy Coulomb excitation, due to the high bombarding energy, care must be taken to exclude nuclear contributions to the electromagnetic excitation process. This was accomplished by restricting the analysis to events at very forward scattering angles, which correspond to large impact parameters, b. In this case, scattering angle upper limit cuts were made to ensure $b > b_{min} = 1.2(A^{1/3}_{target} + A^{1/3}_{projectile}) + 2$ fm [21]. Using the mid-target beam energies, this requirement corresponded to angle cuts of $\Theta^{max}_{lab} = 2.3°$, 2.5°, 2.2° and 2.1° for the ^{66}Fe thin target, the ^{66}Fe thick target, ^{68}Fe and ^{64}Cr, respectively.

The reaction target in front of the S800 spectrograph was surrounded by CAESAR, an array of 192 CsI(Na) scintillator crystals for γ-ray detection [22]. The high granularity of the array allowed for an event-by-event Doppler reconstruction, where the angle of the emitted γ ray was determined based on the position of the crystal recording the highest energy deposition in a given event. Covering approximately 95% of the solid angle, the singles photo-peak efficiency of CAESAR was determined to be 30% at 1 MeV. Energy calibrations and photopeak efficiencies were determined with standard ^{22}Na, ^{60}Co, ^{137}Cs and ^{88}Y sources, and compared with GEANT4 simulations which were used to model the response of the array. The simulations reproduced the measured source efficiencies of the set-up to within 3%, which is included as a systematic error in the results.

The event-by-event Doppler-corrected γ-ray spectra obtained in coincidence with ^{66}Fe (245.2 mg/cm^2 target thickness), ^{68}Fe and ^{64}Cr, satisfying the safe Coulomb excitation angle requirement, are shown in Figure 1. In each case, the only observed peak was the $2^+_1 \rightarrow 0^+_1$ transition, and the energies of these transitions agree well with the literature values [10–12]. To extract the number of γ rays emitted in each case, fits of the results of a GEANT4 simulation to the data were performed. The simulations account for the efficiency response of CAESAR, absorption in the target and include the calculated

γ-ray angular distribution for the Coulomb excitation process [23, 24]. Overlaid on the experimental spectra in Figure 1 are the results of the fit, which included the GEANT4 simulated response function, plus a sum of two exponentials to represent the smooth background.

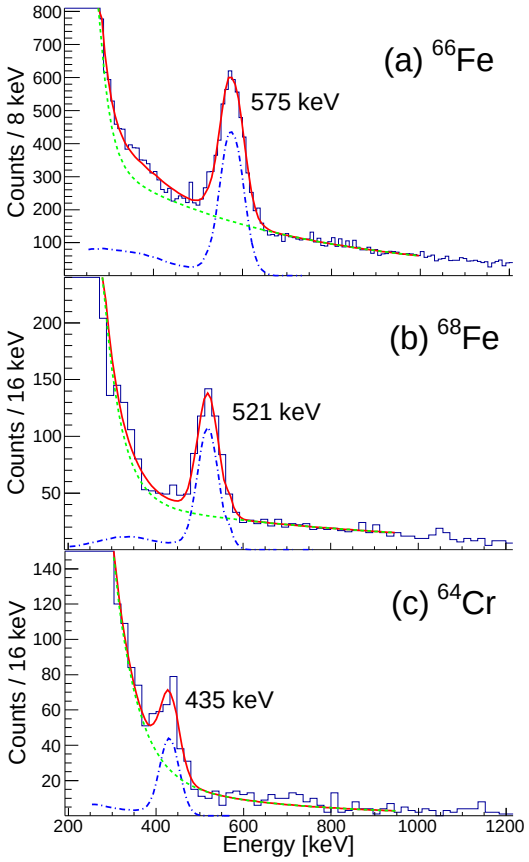

FIG. 1: (Color online) Doppler-corrected gamma-ray spectra collected in coincidence with (a) ^{66}Fe, following Coulomb excitation on the thin 245 mg/cm^2 ^{209}Bi target, (b) ^{68}Fe and (c) ^{64}Cr. In each case, the spectra include gamma rays in coincidence only with events detected in the S800 focal plane, and scattering angles below the cut-off determined for safe impact parameters as described in the text. The fit of the GEANT simulation output (dot-dashed blue line) plus double exponential background (dashed green line) is shown in each case by the solid red line.

Angle-integrated Coulomb excitation cross sections to the first 2^+ were determined and translated into $B(E2; 0_1^+ \rightarrow 2_1^+)$ values based on relativistic Coulomb excitation calculations performed following the formalism of Alder and Winther [24], using RELEX [25]. The Coulomb excitation cross-sections, and extracted $B(E2)$ values are presented in Table I. The excitation cross-sections include statistical uncertainties, uncertainties due to the fitting procedure used to extract the number of γ rays, and uncertainties in the simulated vs. measured array efficiencies of 3% as described previously. In the case of ^{64}Cr, the error in the simulated vs. measured array response was estimated to be 6%, due to the low-energy of the $2_1^+ \rightarrow 0_1^+$ transition, the sensitivity of the array response to detector thresholds and the lack of a calibration point below 511 keV. The extracted $B(E2)$ values include an additional 5% uncertainty arising from the reconstruction of the scattering angle. The total error on the $B(E2)$ values presented in Table I results from summing the contributing uncertainties in quadrature.

TABLE I: Angle-integrated Coulomb excitation cross-sections, and extracted $B(E2; 0_1^+ \rightarrow 2_1^+)$ values for ^{66}Fe (both target thicknesses), ^{68}Fe and ^{64}Cr.

Isotopes	Target (mg/cm^2)	σ (mb)	$B(E2\uparrow)$ (e^{2}fm^4)	Previous (e^{2}fm^4)	LNPS (e^{2}fm^4)
$^{66}_{26}$Fe	245.2	318(22)	1455(124)	1660(170) [14]	1680
	492	331(30)	1430(149)		
$^{68}_{26}$Fe	245.2	388(43)	1777(216)	–	1845
$^{64}_{24}$Cr	492	333(83)	1561(396)	–	1805

The present results confirm the previous RDM lifetime measurement and $B(E2)$ value in ^{66}Fe$_{40}$ as determined by Rother *et al.* [14], with excellent agreement between the $B(E2)$ values determined using the two different ^{209}Bi target thicknesses in the present measurement. The present results also extend the measured $B(E2)$ values for the Fe isotopic chain to N=42 (^{68}Fe), and provide the first result at N=40 in the $_{24}$Cr chain.

Large-scale shell model calculations provide one theoretical description of the region of N=40, and have been successful in describing the low-energy structure of upper pf-shell nuclei. The Lenzi-Nowacki-Poves-Sieja (LNPS) effective interaction [7] assumes a ^{48}Ca core, and a valence space including the full pf shell for protons, and the $1f_{5/2}$, $2p_{3/2}$, $2p_{1/2}$, $1g_{9/2}$ and $2d_{5/2}$ single-particle states for neutrons. The interaction is tuned to reproduce the N=50 shell closure behaviour as observed in the $_{40}$Zr isotopic chain, and has shown good agreement with the excitation energies and $B(E2)$ values for the Fe and Cr isotopes approaching N=40. The shell-model results using the LNPS effective interaction as presented in Ref. [7] are shown together with available experimental data down to N=32 in Fig. 2, including the present results.

As is evident in the top panel of Fig. 2, the LNPS effective interaction reproduces the energy of the first 2^+ excited states in the Fe and Cr chains quite well. However, the shell-model calculations appear to overestimate the magnitude of the quadrupole transition strengths using the standard polarization charge of 0.5e [8]. Using instead more realistic effective charges according to the Bohr-Mottelson formulation of the polarization charges, which include isovector and isoscalar components [29], the magnitudes of the calculated $B(E2)$ values are systematically reduced and the agreement of the calculated values with the experimental

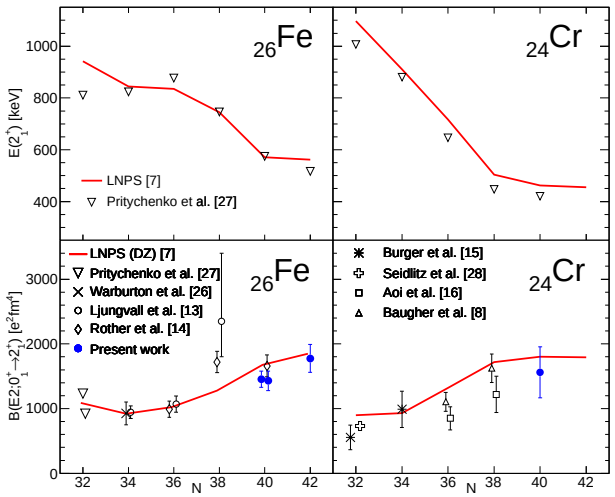

FIG. 2: (Color online) Systematics of $E(2_1^+)$ (upper panels) and quadrupole collectivity(lower panels) along the Fe (left panels) and Cr (right panels) isotopic chains. Shell-model calculations using the state-of-the-art LNPS [7] effective interaction are shown by the solid red lines, using the effective charges of Dufour and Zuker [30], and the nucleon valence spaces as described in the text for N=34 through N=42. For the calculations at N=32, the neutron valence space excluded the $1g_{9/2}$ and $2d_{5/2}$ orbitals, but included the entire pf shell required for description of the lighter isotopes. Available experimental data are shown in hollow black symbols, including results deduced, with an optical model dependence, from (p,p') measurements [16]. The present results are shown as filled blue circles.

results, including the present result at ^{64}Cr, are improved. Alternatively, recent investigations have shown that the use of the effective charges deduced by Dufour and Zuker [30], i.e. $e_\pi = 1.31e$ and $e_\nu = 0.46e$, without the need of including an isovector component, give an excellent description of the transition probabilities in different mass regions [31] and are compatible with the ones obtained in a recent fit of E2 properties of the *sd*-shell with the USDA interaction [32]. We therefore adopt these effective charges and report the shell-model predictions shown by the solid red line in the bottom panels of Fig. 2.

It is worth emphasizing the importance of including the neutron $2d_{5/2}$ orbit in the valence space of the shell model calculations, as is done in the calculations presented using the LNPS effective interaction. The inclusion of this orbital, a member of the quasi-SU3 sequence also containing the $1g_{9/2}$ orbit, is critical to building the quadrupole collectivity in the neutron-rich Fe and Cr isotopes [7], which calculations excluding this state fail to reproduce [33].

It is also interesting to note that the while no conclusions can be drawn looking at all available data, the present results suggest larger collectivity in ^{68}Fe$_{42}$ with respect to ^{66}Fe$_{40}$. The trend in the theoretical predictions is the same, but smoother. In order to conclude that a nucleus has permanent deformation, it is necessary that both the $B(E2)$'s of the yrast band and the spectroscopic quadrupole moments can be obtained, to a very good approximation, from a single intrinsic deformed state. This is indeed the case in the calculations; for instance in ^{64}Cr this requirement is satisfied at the 3% level. The theoretical results can be interpreted in terms of the proton and neutron $E2$ transition amplitudes A_π and A_ν. The $B(E2)$ values and the intrinsic quadrupole moments are obtained from these transition amplitudes by the expressions [7, 8]:

$$B(E2 : 2_1^+ \rightarrow 0_1^+) = (e_\pi A_\pi + e_\nu A_\nu)^2 \qquad (1)$$

$$Q_0 = \sqrt{16\pi\ B(E2\downarrow)} = \sqrt{16\pi}(e_\pi A_\pi + e_\nu A_\nu) \qquad (2)$$

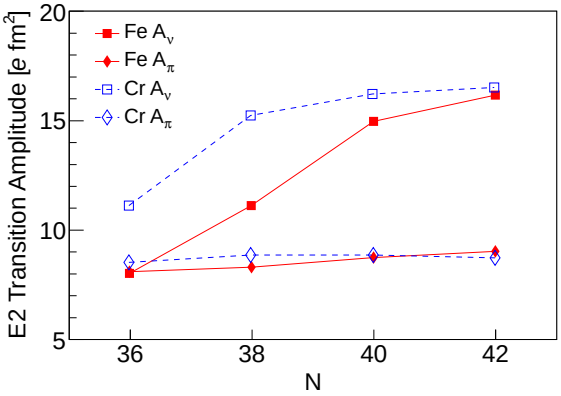

FIG. 3: (Color online) Calculated proton and neutron electric quadrupole ($2_1^+ \rightarrow 0_1^+$) transition amplitudes, in e fm^2.

As can be seen in Figure 3, the proton contribution to the $B(E2)$ values both in Cr and Fe isotopes is essentially constant, while the neutron contribution increases through N=38 in the Cr isotopic chain. In the case of the Fe isotopes, the neutron contribution increases through N=40, reproducing rather well the increase in $B(E2)$ value observed moving from ^{66}Fe to ^{68}Fe. Another point of note is that the measured $B(E2)$ value of ^{68}Fe is slightly larger than that of ^{64}Cr, also in agreement with theory, although the error bars do not allow for a definite conclusion.

However the issue of collectivity depends very much on the criteria chosen to gauge it. A measure of the "nuclear" collectivity is given by the intrinsic mass quadrupole moment:

$$Q_0(mass) = \sqrt{16\pi}\ q_m(A_\pi + A_\nu) \qquad (3)$$

to which neutrons and protons contribute with the same weight. With the effective mass q_m=1.77 (the sum of the proton and neutron effective charges) and normalizing the calculated Q_0's to A=64 to remove the $A^{5/3}$ dependence of Q, within the framework of the shell model calculations, we obtain intrinsic mass quadrupole moments

of 273, 318, 313 and 300 fm^2 for $^{60-66}$Cr, and 214, 243, 281 and 284 fm^2 for $^{62-68}$Fe. These calculations show a saturation of the deformation at N=38 in the Cr chain, and at N=40 in the Fe isotopes, as was noted in Ref. [7]. Although marginally so, $^{62-64}$Cr are calculated to be the most deformed members of the island from the nuclear matter point of view, with β=0.3, while in both the experiment and calculations ^{68}Fe has the largest $B(E2)$ value and electric intrinsic quadrupole moment.

In summary, we have studied the quadrupole collectivity in the neutron-rich $N\sim$40 nuclei ^{66,68}Fe and ^{64}Cr via intermediate energy Coulomb excitation. The present results provide a direct measure of the $B(E2; 0_1^+ \rightarrow 2_1^+)$ for the first time in ^{68}Fe$_{42}$ and ^{64}Cr$_{40}$, and confirm a previous RDM lifetime measurement in ^{66}Fe$_{40}$. These new data in the most neutron-rich Fe and Cr isotopes provide a stringent test for state-of-the-art shell model theory. Comparison with calculations using the LNPS effective interaction show that the overall trend in $B(E2)$ values is well reproduced using realistic, universal effective charges. The calculations also show that nuclei in this region are well deformed, with maximum deformation in $^{62-64}$Cr, or ^{68}Fe, depending on the criteria chosen to define deformation. Extension of the $B(E2)$ systematics in this region, particularly in the $_{22}$Ti isotopic chain below Cr, will be of interest as these isotopes become experimentally accessible, to confirm the true center of this region of deformation. Likewise, reaching further in neutron number towards the N=50 spherical shell closure in the Cr and Fe isotopes will provide critical tests of the most advanced theoretical calculations.

This work was supported by the National Science Foundation under Grant No. PHY11-02511 (NSCL), and by the U.S. Department of Energy under contract No. DE-AC02-05CH11231 (LBNL) , No. DE-FG02-08ER41556 (NSCL) and under grant No. DE-FG52-06NA26206 and No. DE-FG02-05ER41379 (University of Richmond). Part of this work was performed under the auspices of the U.S. Department of Energy Lawrence Livermore National Laboratory (LLNL) under contract No. DE-AC52-07NA27344. A. Poves recognizes MICINN (Spain) (FPA2011-29854) and Comunidad de Madrid (Spain) (HEPHACOS S2009-ESP-147) for support. We would also like to thank the operations staff at NSCL for their outstanding work in beam delivery.

[1] M. G. Mayer, Phys. Rev. **75**, 1969 (1949).
[2] O. Haxel, J. H. D. Jensen, H. E. Suess, Phys. Rev. **75**, 1766 (1949).
[3] T. Otsuka, T. Suzuki, R. Fujimoto, H. Grawe, and Y. Akaishi, Phys. Rev. Lett. **95**, 232502 (2005).
[4] E. K. Warburton, J. A. Becker and B. A. Brown, Phys. Rev. C **41**, 1147 (1990).
[5] B. R. Mottelson and S. G. Nilsson, Phys. Rev. **99**, 1615 (1955).
[6] A. P. Zuker, J. Retamosa, A. Poves, and E. Caurier, Phys. Rev. C **52**, R1741 (1995).
[7] S. M. Lenzi, F. Nowacki, A. Poves, and K. Sieja, Phys. Rev. C **82**, 054301 (2010).
[8] T. Baugher *et al.*, Phys. Rev. C **86**, 011305(R) (2012).
[9] O. Sorlin *et al.*, Eur. Phys. J. A **16**, 55 (2003).
[10] A. Gade, *et al.*, Phys. Rev. C **81**, 051304(R) (2010).
[11] M. Hannawald *et al.*, Phys. Rev. Lett. **82**, 1391 (1999).
[12] P. Adrich *et al.*, Phys. Rev. C **77**, 054306 (2008).
[13] J. Ljungvall *et al.*, Phys. Rev. C **81**, 061301(R) (2010).
[14] W. Rother *et al.*, Phys. Rev. Lett. **106**, 022502 (2011).
[15] A. Bürger, *et al.*, Phys. Lett. B **622**, 29 (2005).
[16] N. Aoi *et al.*, Phys. Rev. Lett **102**, 012502 (2009).
[17] T. Glasmacher, Ann. Rev. Nucl. Part. Sci. **48**, 1 (1998).
[18] D. J. Morrissey *et al.*, Nucl. Instrum. Methods Phys. Res. B **204**, 90 (2003).
[19] D. Bazin *et al.*, Nucl. Instrum. Methods Phys. Res. B **204**, 629 (2003).
[20] J. Yurkon *et al.*, Nucl. Instrum. Methods Phys. Res. A **422**, 291 (1999).
[21] A. Gade *et al.*, Phys. Rev. C **68**, 014302 (2003).
[22] D. Weisshaar *et al.*, Nucl. Instrum. Methods Phys. Res. A **624**, 615 (2010).
[23] H. Olliver, T. Glasmacher and A. E. Stuchbery, Phys. Rev. C **68**, 044312 (2003).
[24] A. Winther and K. Alder, Nucl. Phys. A **319**, 518 (1979).
[25] C.A. Bertulani, Computer Physics Communications **116**, 345 (1999).
[26] E. K. Warburton, J. W. Olness, A. M. Nathan, J. J. Kolata and J. B. McGrory, Phys. Rev. C **16**, 1027 (1977).
[27] B. Pritychenko, J. Choquette, M. Horoi, B. Karamy and B. Singh, At. Data Nucl. Data Tables **98**, 798 (2012), and references therein.
[28] M. Seidlitz *et al.*, Phys. Rev. C **84**, 034318 (2011).
[29] A. Bohr and B. R. Mottelson, *Nuclear Structure*, Vol. 2 (Benjamin, New York, 1975).
[30] M. Dufour and A. P. Zuker, Phys. Rev. C **54**, 1641 (1996).
[31] F. Nowacki, private communication
[32] W. A. Richter, S. Mkhize and B. A. Brown, Phys. Rev. C **78**, 064302 (2008).
[33] E. Caurier, F. Nowacki and A. Poves, Eur. Phys. J. A **15**, 145 (2002).